Biomaterials xxx (2013) 1–10

Contents lists available at SciVerse ScienceDirect

Biomaterials

journal homepage: www.elsevier.com/locate/biomaterials

Predicting the therapeutic efficacy of MSC in bone tissue engineering using the molecular marker CADM1

Anouk Mentink [a], Marc Hulsman [b], Nathalie Groen [a], Ruud Licht [a], Koen J. Dechering [c], Johan van der Stok [d], Hugo A. Alves [a], Wouter J. Dhert [e], Eugene P. van Someren [b], Marcel J.T. Reinders [b], Clemens A. van Blitterswijk [a], Jan de Boer [a,*]

[a] University of Twente, MIRA Institute for Biomedical Technology and Technical Medicine, Department of Tissue Regeneration, Drienerlolaan 5, 7522 NB Enschede, The Netherlands
[b] Delft Bioinformatics Lab, Faculty of Electrical Engineering, Mathematics and Computer Science, Delft University of Technology, Delft, The Netherlands
[c] Pharmacology Department, Schering-Plough Research Institute, Oss, The Netherlands
[d] Orthopedic Research Laboratory, Department of Orthopaedics, Erasmus MC, University Medical Center Rotterdam, Rotterdam, The Netherlands
[e] Translational Musculoskeletal Research, University Medical Center Utrecht, Division of Surgical Specialties, Dept. Orthopaedics, Utrecht, The Netherlands

ARTICLE INFO

Article history:
Received 8 January 2013
Accepted 1 March 2013
Available online xxx

Keywords:
Bone tissue engineering
Mesenchymal stromal cells
Diagnostic marker
Gene expression profiling
CADM1

ABSTRACT

Mesenchymal stromal cells (hMSCs) are advancing into the clinic but the therapeutic efficacy of hMSCs faces the problem of donor variability. In bone tissue engineering, no reliable markers have been identified which are able to predict the bone-forming capacity of hMSCs prior to implantation. To this end, we isolated hMSCs from 62 donors and characterized systematically their *in vitro* lineage differentiation capacity, gene expression signature and *in vivo* capacity for ectopic bone formation. Our data confirms the large variability of *in vitro* differentiation capacity which did not correlate with *in vivo* ectopic bone formation. Using DNA microarray analysis of early passage hMSCs we identified a diagnostic bone-forming classifier. In fact, a single gene, *CADM1*, strongly correlated with the bone-forming capacity of hMSCs and could be used as a reliable *in vitro* diagnostic marker. Furthermore, data mining of genes expressed correlating with *in vivo* bone formation represented involvement in neurogenic processes and Wnt signaling. We will apply our data set to predict therapeutic efficacy of hMSCs and to gain novel insight in the process of bone regeneration. Our bio-informatics driven approach may be used in other fields of cell therapy to establish diagnostic markers for clinical efficacy.

1. Introduction

Many human diseases are caused by failure of tissue function, with well-known examples such as diabetes, damage inflicted by myocardial infarcts and degeneration of the hip joint. The disciplines of tissue engineering and cell therapy aim at restoring worn-out or diseased tissues for which the patient's own body represents a source of autologous cells [1]. For instance, a much used source of autologous cells in the field of bone tissue engineering is human multipotent mesenchymal stromal cells (hMSCs), also referred to as mesenchymal stem cells [2]. Because hMSCs can be easily isolated from bone marrow aspirates and expanded *in vitro*, they are used for various cell-based therapeutic applications [3]. hMSCs are multipotent cells which are able to differentiate, depending on the stimulus, into several lineages including the osteogenic, chondrogenic and adipogenic lineage *in vitro* [4]. Osteogenic differentiation of hMSCs is characterized by expression of alkaline phosphatase (ALP) and the formation of a mineralized extracellular matrix (ECM) containing hydroxyapatite. Molecules such as dexamethasone (dex), 3′-5′-cyclic adenosine monophosphate (cAMP), 1,25-dihydroxyvitaminD (vitD3) and bone morphogenetic protein 2 (BMP-2) are used to drive osteogenic differentiation of hMSCs *in vitro* [5–7]. For bone tissue engineering, we and others have demonstrated ectopic bone formation by seeding hMSCs onto porous calcium phosphate scaffolds and subsequent subcutaneous implantation into immune-deficient mice [8,9]. Although proof of principle exists for bone tissue engineering in animal models [10], clinical application is hampered by large donor variation in the ability of hMSCs to deposit bone tissue *in vivo* [11,12]. Unfortunately, bone tissue engineering efficacy is not correlated to known clinical or molecular labels. This is partly due to the fact that the field of hMSC biology lacks an elaborate classification system of CD markers to define stem cells, progenitor

* Corresponding author. Tel.: +31 534895791; fax: +31 534892150.
E-mail address: j.deboer@tnw.utwente.nl (J. de Boer).

0142-9612/$ – see front matter © 2013 Elsevier Ltd. All rights reserved.
http://dx.doi.org/10.1016/j.biomaterials.2013.03.001

cells and differentiated cells as it is known for the hematopoietic stem cell system. Cell surface markers such as Stro-1 and the nerve growth factor receptor have been used to prospectively isolate clonogenic hMSCs from a crude bone marrow aspirate [13,14], but the resultant population of cells is still heterogenic in its biological performance. CD146 defines an hMSC subpopulation with the ability to organize a hematopoietic niche *in vivo* but its expression on hMSCs does not correlate to bone formation per se [15]. Therefore, it would be beneficial to define diagnostic markers in culture expanded hMSCs which can predict their *in vivo* performance. The markers could be used to select patients eligible for clinical trials but also provide biological tools to interfere with the osteogenic potential of hMSCs.

The use of diagnostic markers for tissue engineering outcome is successfully used in the field of cartilage regeneration, where Dell'Accio et al. identified a set of molecular markers predictive for *in vivo* cartilage formation of adult human articular chondrocytes [16]. The genes were identified based on their known involvement in the chondrogenic process and similarly, we and others have tried to correlate the expression of genes involved in the osteogenic process in hMSCs to their potency to form bone *in vivo*. Although correlations were found between collagen type I and osteoprotegerin [17] or ALP expression [18] and bone formation, the data sets used were too small to firmly establish a link between gene expression and bone formation and no new insight in the process was obtained. To this end, larger data sets are required for which genome-wide gene expression profiling can be applied. Recently, Larsen et al. identified a molecular phenotype for hMSCs with *in vivo* bone-forming capacity by comparing low versus high bone-forming hMSC-TERT cell populations [19]. Also, in the same group Burns et al. described a correlation between *in vivo* bone formation and *in vitro* expression of matrix proteins determined by analysis of the same cell populations in three-dimensional hydroxyapatite-tricalcium phosphate osteospheroid cultures [20]. However, in both cases donor-to-donor variation is not taken into account since both cell populations originate from the same donor, and thus the molecular signature of bone-forming hMSCs remains incomplete.

We have previously reported on a microarray based approach to distinguish metastasizing from non-metastasizing breast tumors starting from RNA isolated from a breast tumor biopsy [21]. In this study, we have used a similar strategy to find *in vitro* diagnostic markers which are able to predict the *in vivo* bone-forming capacity of hMSCs. We developed a bank of hMSCs from 62 different donors, performed various *in vitro* differentiation assays and analyzed the *in vivo* bone formation for each donor. In addition, we determined the gene expression profile of the hMSCs from the different donors and correlated it with the *in vivo* bone-forming capacity (outlined in Fig. 1). In this manuscript, we present a molecular signature of bone-forming hMSCs.

2. Materials and methods

2.1. Isolation and culture of hMSCs

Bone marrow aspirates (5–20 mL) were obtained from donors with written informed consent, and hMSCs were isolated and proliferated as described previously [22]. Briefly, aspirates were resuspended using a 20-gauge needle, plated at a density of 500,000 cells/cm^2 and cultured in hMSC proliferation medium containing α-MEM (Gibco), 10% heat-inactivated fetal bovine serum (Biowhittaker), 0.2 mM ascorbic acid (Sigma), 2 mM L-glutamine (Gibco), 100 U/mL penicillin with 100 mg/mL streptomycin (Gibco) and 1 ng/mL basic fibroblast growth factor (Instruchemie, Delfzijl, The Netherlands). The serum batch was selected based on proliferation rate and osteogenic differentiation potential. Cells were grown in a humid atmosphere with 5% CO_2. After plating of the bone marrow aspirate, the cells obtained from the first trypsinization were considered as PD (population doubling) 0. Relative population doublings refers to the number of population doublings that cells had undergone, relative to PD 0. Basic medium was composed of proliferation medium without basic fibroblast growth factor, osteogenic medium was composed of basic medium supplemented with 10^{-8} M dex (Sigma) and mineralization medium was composed of basic medium supplemented with 10^{-8} M dex and 0.01 M β–glycerophosphate (Sigma). After expansion, cells of the same batch were split into the different media for differentiation assays.

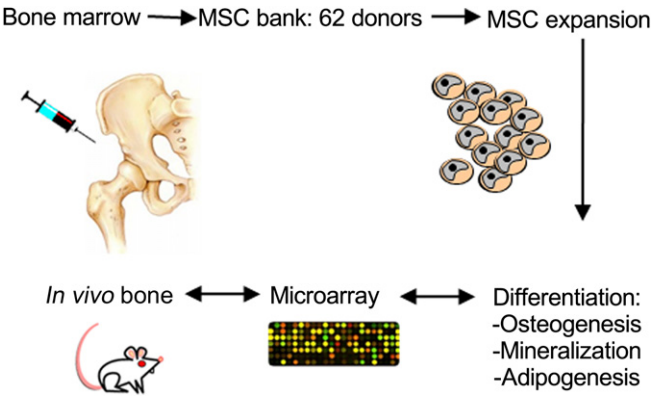

Fig. 1. Study outline. Bone marrow aspirates were obtained from 62 donors, hMSCs were isolated and expanded, subsequently the *in vivo* bone formation, microarray expression profile and differentiation capacity of the cells were determined.

2.2. In vivo bone formation

To evaluate the bone-forming capacity of hMSCs, cells were seeded onto porous biphasic calcium phosphate (BCP) ceramic granules of approximately 2–3 mm, prepared and sintered at 1150 °C as described previously [23]. In total, 200,000 cells per three particles were seeded, in osteogenic medium. This seeding density is on the lower hand to avoid an outcome of 100% bone-forming donors. After one week of culturing, tissue-engineered constructs were implanted subcutaneously in immune-deficient mice (Hsd-cbp:NMRI-nu, Harlan, $n = 6$ for each donor). The mice were anesthetized by intramuscular injection of 0.05 mL of 0.5 mg/mL of anesthetic (1.75 mL of 100 μg/mL ketamine, 1.5 mL of 20 mg/mL xylazine and 0.5 mL of 0.5 mg/mL atropine). Four subcutaneous pockets were made dorsally and each pocket was implanted with three particles. Animals were housed at the Central Laboratory Animal Institute (Utrecht University, Utrecht, The Netherlands), and experiments were approved by the local animal care and use committee. After six weeks, the mice were sacrificed using CO_2 and samples were explanted, fixed in 1.5% glutaraldehyde (Merck) in 0.14 M cacodylic acid (Fluka) buffer (pH 7.3), dehydrated and embedded in methyl methacrylate (LTI) for sectioning. Sections were processed on a histological diamond saw (Leica SP1600). Sections were etched with an HCl/ethanol mixture and sequentially stained to visualize bone, with 1% methylene blue (Sigma) and 0.03% basic fuchsin (Sigma), which stained cells blue and bone pink. Histomorphometry was performed by making low-magnification images from three sections per sample, with a standard selection procedure for each donor. In short, one section in the middle of the scaffold was chosen and the other two sections (left and right side) imaged had the same spacing from the middle section. Scaffold and bone were pseudo colored, and image analysis was performed with KS400 software (Zeiss Vision). A custom-made program (University of Utrecht) was used to measure percentage of bone area compared to scaffold area.

2.3. Mineralization

To determine the mineralization capacity and calcium deposition, hMSCs were seeded in T25 flasks at 5000 cells/cm^2. Cells were cultured in mineralization medium for three weeks, in triplicate. The total calcium deposition was analyzed by using a Calcium Assay Kit (Quantichrom, BioAssay Systems) according to manufacturer's protocol. Briefly, 0.5 N HCl was used to release calcium and the calcium content was measured at 620 nm and expressed as mg/dl.

2.4. Adipogenesis

Adipogenic differentiation capacity of hMSCs was determined as described previously [24]. In short, after three weeks of culture in adipogenic medium, lipid formation was visualized by staining with Oil red O and staining was quantified by extraction of color and measuring absorbance at 540 nm.

2.5. Chondrogenesis

Cells were grown in pellet culture for 21 days with 250,000 cells/pellet in serum-free chondrogenic medium containing TGFβ3 [25]. Chondrogenic medium was supplemented with 250 ng/mL human BMP6 (Biovision) [26]. Pellets were fixed and stained with Alcian Blue (Sigma).

Please cite this article in press as: Mentink A, et al., Predicting the therapeutic efficacy of MSC in bone tissue engineering using the molecular marker CADM1, Biomaterials (2013), http://dx.doi.org/10.1016/j.biomaterials.2013.03.001

2.6. Flow cytometry

To analyze ALP expression and expression of CD markers, we used flow cytometry as described previously [24]. For measuring ALP expression, a 1:50 dilution of primary antibody was used (anti-ALP, B4-78, Developmental Studies Hybridoma Bank, University of Iowa) and a 1:100 dilution of secondary antibody (goat-anti-mouse IgG PE, R&D Systems). For cell surface markers, the same procedure was performed using antibodies for CD105, CD11b, CD19, CD45, HLA-DR, CD90 (R&D Systems), CD73 and CD34 (AbCam).

2.7. Western blotting

hMSCs were grown in proliferation medium and hSCLC cells (GLC4, kindly provided by the Department of Medical Oncology, University Medical Center Groningen) were grown in RPMI1640 (Gibco) supplemented with 10% heat-inactivated fetal bovine serum (Biowhittaker) and 100 U/mL penicillin with 100 mg/mL streptomycin (Gibco). Total protein was isolated and quantified using the BCA protein assay kit (Pierce). Cell lysates were separated using sodium dodecyl sulfate polyacrylamide gel electrophoresis and transferred to an Immobilon-P membrane. The membrane was blocked in Tris-buffered saline with 5% milk for 1 h and probed with 0.1 μg/mL polyclonal anti-CADM1 (Santa Cruz, sc-33198), overnight at 4 °C. Next, the membrane was incubated with horseradish peroxidase conjugated goat anti-rabbit IgG (Dako) as the secondary antibody for 1 h at RT. Protein detection was performed by luminescence, using a Kodak image station 4000 MM after incubating the membranes with Supersignal chemiluminescent detection (Pierce) for 2 min.

2.8. Immunofluorescence

hMSCs were seeded and when reaching 60% confluence fixed with 10% formalin for 20 min. After blocking with 1% bovine serum albumin they were probed with 50 times diluted polyclonal anti-CADM1 (Santa Cruz, sc-33198) for 1 h at RT. Next, cells were incubated with Alexafluor488 conjugated goat-anti-rabbit IgG (Invitrogen). As a counterstain we used Alexafluor568 conjugated Phalloidin (Invitrogen) and DAPI (Sigma). Cells were imaged using BD Pathway 435 Bioimager (BD Biosciences).

2.9. Microarray analysis and quantitative polymerase chain reaction

To analyze the gene expression profile of hMSCs, cells were seeded at 1000 cells/cm^2 and upon reaching near confluence RNA was isolated using an RNeasy mini kit (Qiagen) and DNase treated on column with 10U RNase free DNase I (Gibco) at 37 °C for 30 min. DNase was inactivated at 72 °C for 15 min. The quality and quantity of RNA was analyzed by gel electrophoresis and spectrophotometrically. For qPCR, we performed cDNA synthesis using the iScript cDNA synthesis kit (Bio-rad) and qPCR was carried out using iQ SYBR Green Supermix (Bio-rad). Primer (Sigma) sequences are depicted in Table S2, as a reference gene we used *GAPDH* or *B2M* (see figure legends). For *GPM6B* we used primers which were commercially available (SA Biosciences, annealing temperature 55 °C). For all other genes we used 3 mM $MgCl_2$ and an annealing temperature of 60 °C. To test significance we use a paired student's *t*-test. For microarray analysis, the RNA was hybridized to the Human Genome U133A 2.0 Array (Affymetrix) and scanned with a GeneChip G3000 scanner (Affymetrix). The microarray experiments were performed in three batches. To normalize the measurements, we used a normalization method which removes hybridization, amplification and array location based technical effects. To determine the most significant genes with respect to a label-set, we determined a (two-sided) *p*-value for each gene using a permutation test. As test statistic we used the significant analysis of microarrays [27] test statistic [28] for class labels and the F-test for continuous labels. In total, for each label-set, we performed 10,000 permutations. Genes were sorted on their estimated *p*-value. For further analysis, we also calculated gene set enrichments using gene sets from the database of molecular signatures (MsigDB) [29]. In addition to this, we trained a classifier for the binary bone label (bone or no bone), predicting if bone formation would occur for a certain donor or not. We applied a Nearest-Mean classifier (available as part of PRTools, [30]), and performance was estimated using leave-one-out cross-validation. The probesets to be used as features were selected by taking those with the highest SAM test statistic value on the training set. To determine the optimal number of probesets an inner leave-one-out cross-validation loop was performed. An area under curve (AUC) score of the Receiver Operating Characteristic (ROC), a widely used standard for describing and comparing the accuracy of diagnostic tests, was constructed by combining results for the different validation sets using the classifier class probability (determined using maximum likelihood posterior probabilities [30]). ROC represents the tradeoff between the false negative and false positive rates for every possible cut-off. AUC is a measure of the probability that a classifier based on this label would rank a randomly chosen positive donor higher than a randomly chosen negative donor, where AUC = 1 is a perfect ranking classifier and AUC = 0.5 depicts complete randomness.

2.10. Micro-CT scanning

To evaluate differences in bone architecture of *CADM1* knockout and wild type mice, femora of each were selected for micro-CT scanning. Micro-CT scans were acquired using the SkyScan 1076 scanner (Kontich, Belgium) with a 9 μm-resolution protocol (50 kV energy, 200 μA current, 1.0 mm Al filter) and reconstructed using NRecon software 1.6 (SkyScan, Kontich, Belgium). With Dataviewer 1.4, a segment of the distal metaphysis (10 mm) was selected as region of interest. To distinguish calcified tissue from non-calcified tissue and noise, the reconstructed grayscale images were segmented by an automated algorithm using local thresholds [31], resulting in a 3D data set consisting of stacked black/white cross-sections. Cortical and trabecular bone were subsequently automatically separated using in-house software. Trabecular architecture of the metaphysic was characterized by determining the trabecular bone volume fraction (BV/TV), which is the ratio of trabecular bone volume over endocortical tissue volume. Connectivity density, structural model index, trabecular thickness and trabecular separation were also calculated.

2.11. CADM1 knockout mice

The femora and skulls from homozygous *CADM1* knockout mice were obtained from RIKEN BioResource Centre (B6.129S6-Cadm1<tm1Momo>, RBRC04063; Japan). The knockout mice were developed by Takashi Momoi as described previously [32] and deposited at the BioResource Centre. Femora were explanted from both knockout and wild type mice of two distinct ages. One group consisted of 8-week old mice (3 knockout and 2 wild type) and the other group consisted of 11-week old mice (4 knockout and 3 wild type). The femora and skull of the mice (C57BL/6J) were explanted and fixed for 24 h in paraformaldehyde and subsequently transferred to PBS. External differences between the knockout samples and wild type were measured. For the skulls, different diameters were compared between the samples. Detailed information about micro-CT scanning can be found in supplementary text S1.

3. Results

3.1. Large inter-donor variability in biological characteristics of hMSCs

To find a predictive marker for bone formation by hMSCs *in vivo* we aspirated bone marrow from either the acetabulum or the iliac crest of 62 donors undergoing orthopedic surgery, 48 of which were female and 15 were male. The age of the donors varied from 17 to 84 years with an average of 56 years. Aspirates were put into culture and the identity of the proliferating hMSCs was confirmed according to the set of standards proposed by the Mesenchymal and Tissue Stem Cell Committee of the International Society for Cellular Therapy [33]. The cells were adherent to plastic (Fig. S1A) and more than 94% expressed CD73 and CD90, 60% expressed CD105, and less than 2% expressed CD45, CD34, CD11b, CD19 and HLA-DR, as measured by flow cytometry in hMSCs isolated from three donors (Fig. S1C). Moreover, we were able to differentiate the cells into the osteogenic, adipogenic and chondrogenic lineage under standard *in vitro* differentiation conditions, as demonstrated by histological staining (Fig. S1B).

To show that donor variability in the bone-forming capacity exists within this set of hMSCs, we used the ectopic bone formation model in immune-deficient mice [6,15,34–36] to quantify ectopic bone formation *in vivo*. To this end, hMSCs of all donors were seeded onto porous calcium phosphate ceramic scaffolds and cultured for one week in osteogenic medium, prior to implantation ($n = 6$). After six weeks, scaffolds were explanted and bone formation was quantified (Fig. S2). Out of 62 donors, 35 did show bone formation ranging from 0.01 to 4.6% of bone area compared to scaffold area demonstrating a large inter-donor variability (Fig. 2E).

To further investigate donor variability, we characterized the hMSCs for a number of cellular parameters, such as proliferation and *in vitro* differentiation. Indeed, we observed large differences in the rate of hMSC proliferation (Fig. 2A) and osteogenic differentiation, indicated by the potency of dexamethasone (dex) to enhance the expression of the early osteogenic marker ALP. As reported by us previously, both basic and dex-induced expression of ALP showed large donor variation [11]. ALP expression in the control group ranged from 0.2 to 39% of ALP positive cells and in the dex-induced group from 0.3 to 47%, with an average of 12% (Fig. 2B, Table S1). Likewise, large donor variation was observed in the

Please cite this article in press as: Mentink A, et al., Predicting the therapeutic efficacy of MSC in bone tissue engineering using the molecular marker CADM1, Biomaterials (2013), http://dx.doi.org/10.1016/j.biomaterials.2013.03.001

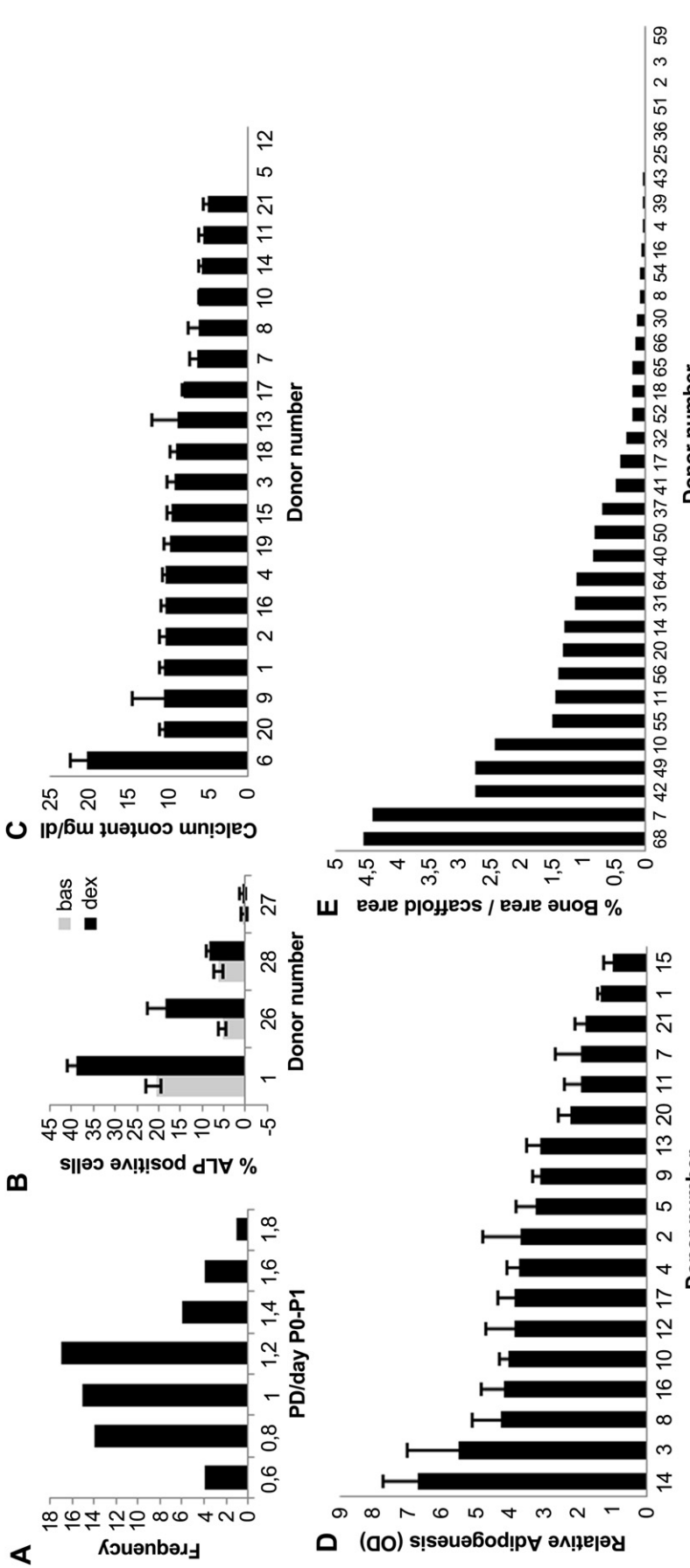

Fig. 2. Characterization of hMSCs. A) Proliferation; hMSCs were cultured and counted when reaching 70–80% confluence. Frequency of population doublings (PD) per day was calculated, passage 0–1, for 61 donors in total. B) ALP expression; hMSCs were cultured in basic (bas) or osteogenic (dex) medium during seven days. The percentage of ALP positive cells was determined using flow cytometry. Error bars represent the standard deviation. Here we show an example for four donors, in Table S1 all values are depicted. C) Mineralization; hMSCs were seeded at 5000/cm^2 and cultured in mineralization medium for three weeks. HCl was used to release calcium and calcium deposition was measured and expressed as mg/dl sample. Error bars represent the standard deviation. D) Adipogenesis; hMSCs were cultured in adipogenic medium for three weeks. Adipogenic differentiation was visualized by staining with Oil red O; the color was extracted and measured spectrophotometrically. Error bars represent the standard deviation. E) *In vivo* bone formation of hMSCs; hMSCs were cultured on BCP particles (200,000 cells/3 particles) in osteogenic medium for seven days and implanted subcutaneously in nude mice for six weeks. Out of 62 donors, 35 showed bone formation. Histomorphometric analysis demonstrated the large variation between donors.

mineralization capacity of hMSCs, which is a late marker for *in vitro* osteogenesis. The ability of the cells to deposit a mineralized matrix ranged from 0 to 20.3 mg/dl of calcium, with an average of 8.3 (Fig. 2C). Similarly, the adipogenic differentiation capacity of hMSCs was determined by quantification of lipid formation after 3 weeks of culture in adipogenic medium. In effect, the optical density (OD) ranged from 1 to 6.7 with an average of 3.3 in 18 different donors (Fig. 2D). In conclusion, the biological performance of hMSCs varied strongly between donors, both *in vivo* and *in vitro*.

3.2. Correlation between cell biological data labels, donor features and bone formation

Differential bone apposition of hMSCs may be correlated to some of the cellular or physiological parameters associated with the hMSCs, as described above, or to the donors from which they were isolated, e.g. gender, age or site of aspiration. Therefore, all available parameters and measured variables were quantitatively correlated to bone formation *in vivo*. As an example, ALP activity is commonly used to describe osteogenic differentiation *in vitro*. It also has been shown previously that hMSCs undergo rapid senescence during *in vitro* culture and lose their ability to differentiate [11].

Consequently, we were interested in assessing the correlation of these parameters and the *in vivo* bone-forming capacity of hMSCs. However, no significant correlation between both ALP expression or proliferation rate of hMSCs and bone formation could be detected (Fig. 3A and B). To further investigate the possibility to use these 2 parameters as a marker able to classify bone-forming versus non bone-forming donors, we produced a Receiver Operating Characteristic (ROC) curve (Fig. 3C). These data indicate that neither ALP activity nor proliferation rate is able to predict the bone-forming capacity of hMSCs *in vivo*. Next, we investigated whether other cell biological features such as number of mononuclear cells per mL of bone marrow, amount of mineralization or adipogenic differentiation, or donor features such as surgery type, site of aspiration, gender or age correlated with the bone-forming capacity. To this end, ROC curves for all these parameters were generated and the areas under curve (AUCs) with corresponding *p*-values were calculated for all labels (Fig. S3A). As can be observed in Fig S3A, significance was not found for any single parameter after

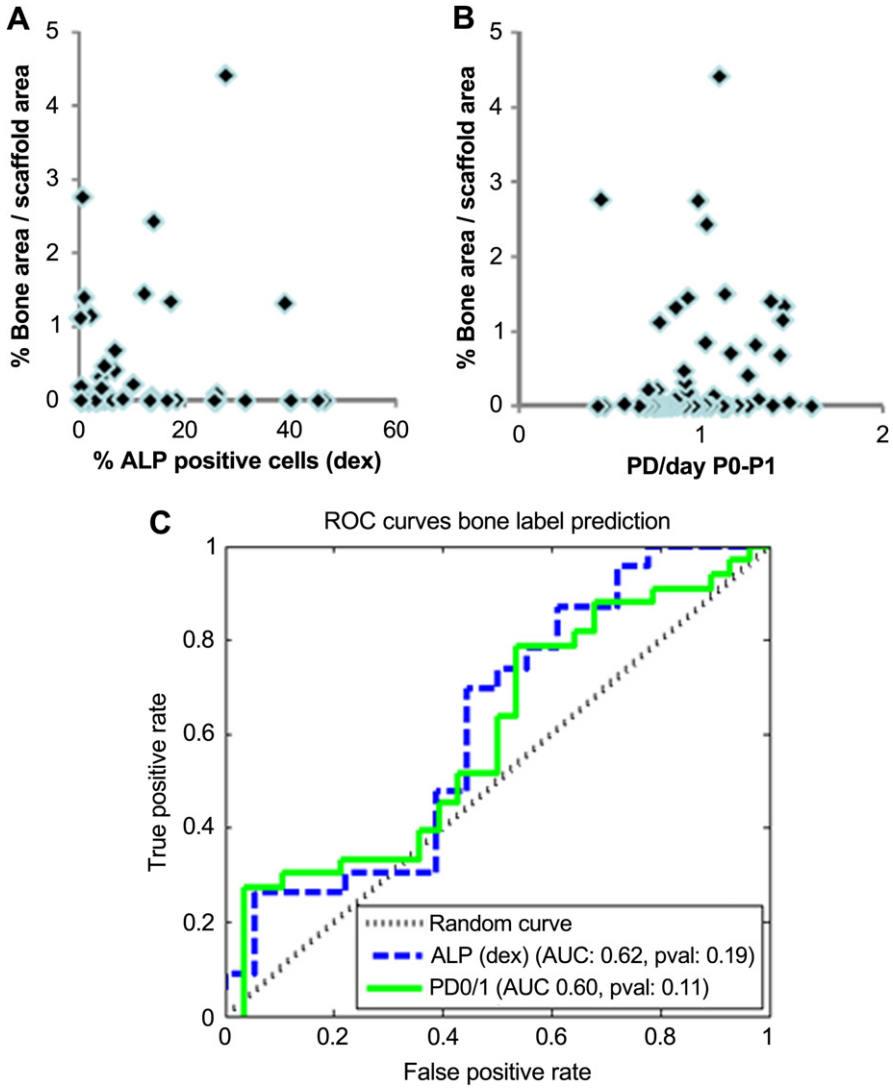

Fig. 3. Correlation between cell biological data labels, donor features and *in vivo* bone formation. A correlation curve was created by plotting the different parameters against the *in vivo* bone formation. An example is shown of percentage of ALP positive cells (dex) (A) or proliferation doublings per day (B). No correlation was found with all data labels. C) Receiver Operating Characteristic (ROC) curves to represent the tradeoff between the false negative and false positive rates for every possible cut-off. The AUC (area under curve) was calculated for all labels, which is a measure of the probability that a classifier based on this label would rank a randomly chosen positive donor higher than a randomly chosen negative donor. The data indicate that neither ALP activity nor proliferation rate correlate with bone-forming capacity *in vivo*.

Please cite this article in press as: Mentink A, et al., Predicting the therapeutic efficacy of MSC in bone tissue engineering using the molecular marker CADM1, Biomaterials (2013), http://dx.doi.org/10.1016/j.biomaterials.2013.03.001

multiple testing correction, neither when the presence or absence of bone was used as a cut-off, nor when the threshold was based on percentage of bone apposition where the amount of bone formed was taken into account. Next, we tried to build a classifier combining both the clinical and biological data, since multiple labels combined may provide a higher predictive value (see Materials and Methods section). The best AUC obtained among all labels for imputation based strategies (i.e. classifier on all donors) was 0.59, which is slightly above random.

3.3. A single gene bone classifier based on whole genome gene expression profiling

Since no cellular or physiological markers could be identified for *in vivo* bone formation by hMSCs, we determined their genome-wide gene expression profile to find genes which' expression could be correlated with *in vivo* bone formation. Therefore, RNA was isolated from undifferentiated hMSCs during the expansion phase in passage two and hybridized to Human Genome U133A 2.0 Arrays (Affymetrix). A diagnostic classifier was built based on the gene expression profiles of the different hMSCs and evaluated on its ability to predict bone-forming capacity. For this purpose, we trained a nearest-mean classifier, using the SAM test statistic to select the genes (see Materials and Methods section). Since we aimed at identifying diagnostic markers able to distinguish bone-forming from non bone-forming donors, only genes displaying a relatively large difference between different hMSCs (standard deviation between arrays > 0.4) were considered. Hence, a list of genes correlating with the *in vivo* bone formation of hMSCs was selected from the remaining 1653 probesets (out of 22,277 genes). Interestingly, in the top 50 of probes (Table 1), 15 genes have been implicated in bone formation before such as *IGF1* [37], *WISP1* [38] and *DKK1* [39] and 11 genes are reported to be implicated in neural adhesion and neuronal functioning such as *CADM1* [40], the neurotransmitter receptor *GABBR2* [41] and carboxypeptidase E [42]. To calculate the predictive value of the probes, ROC curves were created (Fig. 4A), giving the result for different threshold values of the classifier. The best performing classifier showed an AUC score of 0.76, compared to 0.59 for the best clinical classifier. Interestingly, this performance could already be reached using only one probeset (Fig. 4B). We found that in all folds of the cross-validation, the top probe set was the same, which detects the *CADM1* gene. The performance of all *CADM1* probes on the microarray was assessed by calculating the AUC score for each probe (Fig. S4A). Most of the probes showed similar AUC scores, though some of them showed lower values, these were not shown to correlate with possible splice-variants. The *p*-values were calculated (Fig. S4B), showing near significance between the different probes.

Since some factors related to bone formation change their expression before and after the menopause in female donor samples we investigated if this was the case for *CADM1*. As no information is available on the on the onset of the menopause for the donors in this study, we selected all female donors before age 40 as pre-menopause, and female donors after age 61 as post-menopause [43]. This resulted in a set of respectively 10 and 20 donors.

We did not find any significant change in *CADM1* expression between pre-menopause and post-menopause females (ranksum-test *p*-value 0.74). Next, we tested if the strength of the relation of *CADM1* with bone-forming was different for pre-menopause and post-menopause female donors. While we found a substantial difference in AUCs (0.71 versus 0.87), a permutation test did not show this difference to be significant (*p*-value 0.31). In short, while there might be menopause effects, we could not proof this conclusively.

To validate the results obtained by microarray analysis, gene expression data of a number of genes in the top of the gene list was reproduced using quantitative polymerase chain reaction and with these data, ROC curves were created (Fig. 4C). Some of the genes validated by qPCR did show a good correlation with AUCs in the range of the *CADM1* microarray data (which was 0.76) such as the Wnt target gene *WISP1*, with a positive correlation to bone formation (AUC 0.73), *CPE* (AUC 0.72) or the Wnt antagonist *DKK1* with a negative correlation to bone formation (AUC 0.63). Moreover, the positive correlation between bone formation and *CADM1* expression was confirmed by qPCR with an AUC score of 0.84.

To confirm that the CADM1 protein is expressed in hMSCs we performed immunostaining and Western blotting (Fig. S5A). In human small cell lung cancer cells (hSCLC), known to express the CADM1 protein, we observed one band at the expected size of 60 kD. In hMSCs, however, three bands of 60, 75 and 250 kD were observed. The 250 kD and 75 kD bands are most likely post-translationally modified proteins since CADM1 is known to be prone to polysialylation and glycosylation [44]. Immunostaining of CADM1 in hMSCs resulted in a mainly perinuclear appearence of the protein (Fig. S5B).

3.4. Decreased expression of predictive markers upon in vitro expansion

hMSCs lose their multipotency upon *in vitro* expansion [11,45] and specific hMSC markers, such as STRO-1 [46] and NGFR, are known to show concomitant decrease in expression. Therefore, we were interested to analyze the expression of a selection of marker genes from our list, identified to correlate to bone formation, during expansion in six different donors (Fig. 5). The expression of *CADM1* (Fig. 5A) and *CPE* (Fig. 5C) decreased after expansion and interestingly, expression of *DKK1*, which we found to be negatively correlated with bone formation, did increase (Fig. 5B). Expression of other genes in the top list did not change, such as *WISP1* (Fig. 5D), *GPM6B* (Fig. S6A) and *MYO1D* (Fig. S6B). As a control we confirmed that expression of housekeeping genes *β-actin* (Fig. S6C) and *18S* (Fig. S6D) did not change. In conclusion, expansion of hMSCs had an overall negative effect on expression of marker genes correlating with *in vivo* bone formation.

3.5. No distinct bone phenotype in CADM1 knockout mice

Although CADM1 has been associated with a number of biological functions, such as heterotopic cell–cell interaction, this gene has never been related to bone homeostasis. In order to explore this relation, femur bones were explanted from homozygous *CADM1* knockout mice and scanned by micro-CT. Bone mineral density was

Table 1
Genes correlating with *in vivo* bone formation in hMSCs.[a]

Neuronal	Osteogenesis	WNT/IGF-signaling	Miscellaneous/unknown	
CADM1	*HMGA2*	*IGF1*	*CXCR7*	*CRISPLD2*
GABBR2	*S100A4*	*WISP1*	*SEPP1*	*FAM38B*
SEMA5A	*COL14A1*	*DKK1*	*HNMT*	*TXNIP*
GPM6B	*PCOLCE2*	*HOXB7*	*EVI2A*	*ECM2*
CPE	*SOX9*	*WISP2*	*OLFML1*	*PSPH*
ADAM19	*GPM6B*	*SOCS2*	*KCNK2*	*STAT4*
NRN1	*GABBR2*		*PNMAL1*	*LL22NC03-75B3.6*
SHOX2	*SHOX2*		*VCAM1*	*GALNT6*
ENPP2	*OXTR*		*LUM*	*DCN*
OXTR			*IGL*	*IFI44*
MYO1D			*G0S2*	

[a] Top 50 of probes correlating with the *in vivo* bone formation of hMSCs. Some genes were present twice or more since multiple probes per gene were analyzed, these genes are only depicted once in this list.

Please cite this article in press as: Mentink A, et al., Predicting the therapeutic efficacy of MSC in bone tissue engineering using the molecular marker CADM1, Biomaterials (2013), http://dx.doi.org/10.1016/j.biomaterials.2013.03.001

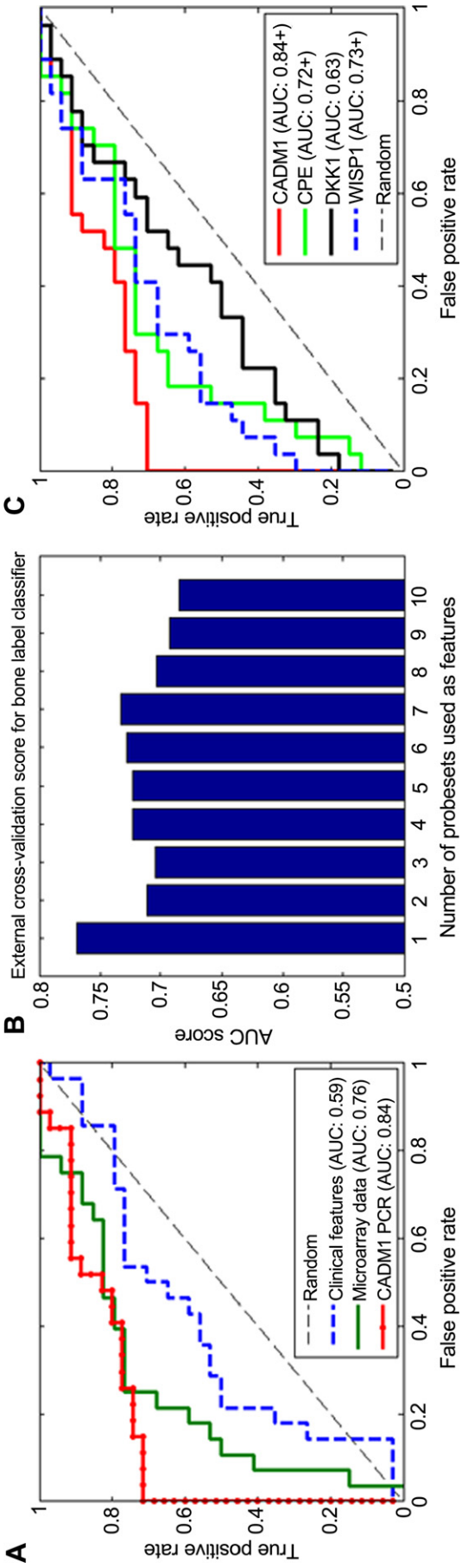

Fig. 4. Classifier performance on the bone labels. Classifier performance on the separation of bone-forming donors from non bone-forming donors. The performance is presented using ROC curves (which represent the tradeoff between false negative and false positive rates for every possible classifier threshold) and the AUC (Area Under ROC curve) score (which represents the probability that the classifier would rank a randomly chosen positive donor higher than a randomly chosen negative donor). A) ROC performance curves of classifiers using either clinical features, microarray probesets or *CADM1* qPCR data (normalized for *GAPDH* expression). ROC curves were obtained by using the posterior probabilities of the validation samples of the leave-one-out cross-validation procedure. Features (probesets) were ranked by using the SAM test statistic within the cross-validation loop. The optimal number of features to select from the top of the ranked list was determined using an inner cross-validation loop. Interestingly, the optimal microarray performance was reached using only one probeset, measuring *CADM1*. No feature selection (and thus cross-validation) was necessary for *CADM1* qPCR. B) AUC score for the microarray data set, using a fixed number of features from the top of the ranked list. The top probeset in every cross-validation fold was *CADM1*. C) qPCR validation of the microarray results (normalized for *GAPDH* expression). Some of the genes were not predictive for bone formation *in vivo*, others did show a good correlation with AUCs in the range of the *CADM1* microarray data.

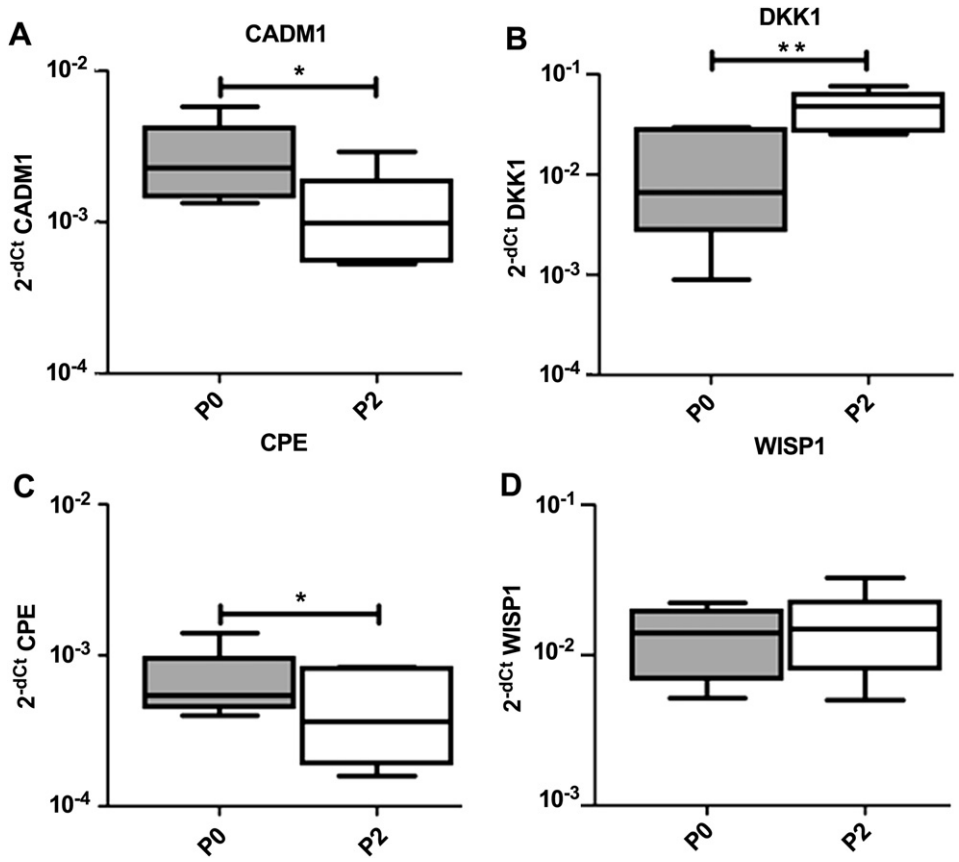

Fig. 5. Expression of predictive markers upon expansion. hMSCs of six different donors were cultured and after passage 0 and 2 RNA was isolated and qPCR was performed (normalized for *B2M* expression) to analyze expression of *CADM1* (A), *DKK1* (B), *CPE* (C) and *WISP1* (D). *CADM1* and *CPE* expression decreased after expansion, and interestingly, *DKK1* expression (wich was negatively correlated to bone formation) increased. Expression of *WISP1* did not change. Error bars represent the standard deviation, for significance a paired student's *t*-test was used ($^{*}p < 0.05$, $^{**}p < 0.01$).

assessed by measuring the bone volume fraction within the endocortical area of the metaphysis region. The bone volume fraction did not differ between the *CADM1* knockout mice and the wild type mice for both 8-week old and 11-week old mice. The other parameters commonly used to distinguish any bone phenotype, such as trabecular separation, trabecular thickness, connectivity density (number of redundant connections between trabecular structures per unit volume), structural model index (prevalence of a particular trabecular shape), also showed no significant changes within the *CADM1* knockout mice (Fig. S7).

4. Discussion

hMSCs have been targeted as potential source for autologous bone tissue engineering almost two decades ago and have been tested in phase 1 clinical trials [47]. Further evaluation is severely hampered by the large donor-to-donor variation in bone apposition. So far, no reliable markers exist that could help sort out "good" from "bad" donors. In our set, we were not able to link bone formation to any of the donor or cellular labels that were analyzed. Using *CADM1* gene expression profiling, we were able to obtain an AUC score of 0.84 for the whole donor set. In practical terms, this means for instance that using *CADM1* expression, we have a tool to include patients into future clinical trials with a high probability of bone apposition. To put this score into perspective, in our experience this is a better performance than what can be obtained with diagnostic marker sets used to distinguish metastatic behavior of breast tumors [48]. It shows that *in vitro* gene expression profiling is an efficient strategy to find diagnostic markers predicting therapeutic efficacy of stem cell therapy. Using a combination of histology and gene expression profiling we have been able to bridge the gap between the expansion of hMSCs in culture and bone apposition *in vivo*. It is important to realize that this approach can be applied in any strategy where the therapeutic efficacy of a stem cell has to be assessed *in vitro*.

Another potential application of *CADM1* lies in the area of drug discovery. The field of bone tissue engineering puts a lot of effort into optimizing the isolation procedures and culture conditions favoring the bone-forming capacity of hMSCs [6,34]. So far, ectopic bone formation *in vivo* is the golden standard to verify the efficacy of a modification to the bone tissue engineering protocol. With *CADM1* as a predictor of bone formation *in vivo*, we can embark on high throughput screening strategies to identify small molecules that improve the bone-forming capacity of hMSCs. Moreover, we can screen libraries of scaffold materials which favor bone formation by hMSCs. Besides screening, the link between *CADM1* and bone formation may shed light on the bone formation process. CADM1 protein is involved in a broad, seemingly pleiotropic range of diseases and functions, such as neuronal synapse formation [40], as a tumor suppressor [49], the communication between mast cells and smooth muscle cells [50] and in venous thrombosis [51]. For example, overexpression of *CADM1* in HEK293 cells resulted in synapse formation in co-cultures with neuronal cells [40]. A common signature may be heterotypic cellular interaction, and the concurrent role of hMSCs as trophic mediators in tissue formation is in line with this. With respect to its neuronal role, it is interesting

to note that in the top 20 of genes associated to bone formation, 11 have a neuronal signature. GABBR2 is a neurotransmitter receptor, SEMA5A is a neuronal adhesion molecule, GPM6B is known to play a role in neurotransmitter release and carboxypeptidase E controls neurotransmitter activity.

Beyond *CADM1*, we identified a number of other genes with a correlation to bone formation and some of them have a known role in the osteogenic process. For instance, IGF1 is known to play a role in the mineralization phase of osteogenesis and controlled release of IGF1 in a bone defect is beneficial to the healing process [52]. We have previously identified IGF1 as a cytokine which is strongly upregulated in hMSCs treated with cAMP [6] and associated with enhanced bone formation as well. Oxytocin is an anabolic bone hormone and together with its receptor OXTR, present in our list, regulates bone mass [53]. SHOX2 has been related to Turner syndrome [54] and as an upstream regulator of *RUNX2* during long-bone development [55]. In fact, the mouse *SHOX2* gene codes for a transcription factor required for the proximal bone formation of the limbs [56]. Moreover, besides its correlation to neuronal functioning, *GPM6B* is reported to be strongly upregulated during osteoblast differentiation and related to alkaline phosphatase activity and matrix mineralization in hMSCs [57]. Similarly, the neurotransmitter receptor GABBR2 is constitutively expressed in murine calvarial osteoblasts and also localized in growth plate and on the membranes of cultured growth plate chondrocytes [58]. GABBR2 was shown to inhibit cAMP formation, ALP activity, and calcium accumulation, and decreases *BMP2*, osteocalcin, and osterix expression. On the other hand, the expression of *ADAM19* was reported in bone-marrow derived mesenchymal stromal cells during chondrogenic differentiation by micropellet culture in the presence of BMP2 [59].

Another group of interesting genes are those involved in Wnt signaling. In the top 100 of genes associated with bone formation, we can find Wnt target genes *WISP1, WISP2* [60], *HOXB7 and S100A4* [61]. *DKK1*, a negative regulator of Wnt signaling [62] on the other hand is negatively associated to bone formation, which is in line with a positive role of Wnt signaling in bone formation. Ironically, we have previously shown that increased Wnt signaling in hMSCs is negatively correlated to osteogenic differentiation of hMSCs *in vitro* but positively correlated to the rate of hMSC proliferation. In that respect, the relatively low *P*-values correlating proliferation rate and bone formation (Fig. S3B) may be due to high Wnt signaling. We are now investigating the effect of Wnt signaling on bone formation *in vivo*.

We show here that expression of predictive markers decreased upon *in vitro* expansion of hMSCs. Interestingly, *DKK1*, which we found to be negatively correlated to ectopic bone formation, showed an increased expression upon expansion. We tested this in six donors and found again a large donor variation. It is also known that both expression of Stro-1, a clonogenic hMSC marker, and *in vivo* bone formation decrease upon expansion [46,63]. For this reason, we are investigating the possibility to directly use the crude bone marrow instead of expanded hMSCs for tissue engineering purposes [64].

Finally, we may isolate the CADM1 positive fraction, preferably from crude bone marrow, and analyze whether the enrichment in percentage of CADM1 positive cells has a beneficial effect on bone formation. Furthermore, the analysis of the CADM1 positive fraction of hMSCs may teach us more about the nature of the bone-forming hMSC. Considering the fact that the ceramics implanted in this study were fully covered by hMSCs, the amount of bone observed was rather low, suggesting that only a small subset of the implanted cells is actually able to enter the osteogenic process. Considering the numerous steps and the long time that separates the moment of gene expression profiling in the expanding hMSCs and histomorphometric assessment of bone formation in nude mice, it is encouraging to see that *CADM1* expression has a high predictive value. Even though very little to nothing is known about the nature of the bone-forming fraction of hMSCs, we have good hopes that the CADM1 positive fraction will shed a light on this process.

5. Conclusions

We have correlated the bone-forming capacity of hMSCs in an immune-deficient mouse model to the expression of genes during the expansion phase of hMSC culture. We have identified the *CADM1* gene as a marker which is able to predict bone formation with an AUC of 0.84. Furthermore, we have disclosed a link between the expression of neurogenic genes and bone-forming capacity of hMSCs. Our approach can be applied in any strategy where the therapeutic efficacy of stem cells needs to be assessed. Furthermore, the *CADM1* gene can be used as a tool for screening small molecules or materials on their effect on bone formation.

Acknowledgments

We thank the Central Laboratory Animal Institute in Utrecht for taking good care of our animals and the Department of Medical Oncology, University Medical Center Groningen for providing us with hSCLC cells. Funding: The authors gratefully acknowledge the support of the Smart Mix Program of the Netherlands Ministry of Economic Affairs and the Netherlands Ministry of Education, Culture and Science (AM, JdB), SenterNovem (JdB, MR, RL, AM, CvB), DPTE (HA, RL) and VIDI (JdB).

Appendix A. Supplementary data

Supplementary data related to this article can be found at http://dx.doi.org/10.1016/j.biomaterials.2013.03.001.

References

[1] Arrington ED, Smith WJ, Chambers HG, Bucknell AL, Davino NA. Complications of iliac crest bone graft harvesting. Clin Orthop Relat Res 1996:300–9.
[2] Bianco P, Robey PG, Simmons PJ. Mesenchymal stem cells: revisiting history, concepts, and assays. Cell Stem Cell 2008;2:313–9.
[3] Caplan AI. Review: mesenchymal stem cells: cell-based reconstructive therapy in orthopedics. Tissue Eng 2005;11:1198–211.
[4] Pittenger MF, Mackay AM, Beck SC, Jaiswal RK, Douglas R, Mosca JD, et al. Multilineage potential of adult human mesenchymal stem cells. Science 1999;284:143–7.
[5] Siddappa R, Fernandes H, Liu J, van Blitterswijk C, de Boer J. The response of human mesenchymal stem cells to osteogenic signals and its impact on bone tissue engineering. Curr Stem Cell Res Ther 2007;2:209–20.
[6] Siddappa R, Martens A, Doorn J, Leusink A, Olivo C, Licht R, et al. cAMP/PKA pathway activation in human mesenchymal stem cells in vitro results in robust bone formation in vivo. Proc Natl Acad Sci U S A 2008;105:7281–6.
[7] de Boer J, Licht R, Bongers M, van der Klundert T, Arends R, van Blitterswijk C. Inhibition of histone acetylation as a tool in bone tissue engineering. Tissue Eng 2006;12:2927–37.
[8] Haynesworth SE, Goshima J, Goldberg VM, Caplan AI. Characterization of cells with osteogenic potential from human marrow. Bone 1992;13:81–8.
[9] de Bruijn JD, van den Brink I, Mendes S, Dekker R, Bovell YP, van Blitterswijk CA. Bone induction by implants coated with cultured osteogenic bone marrow cells. Adv Dent Res 1999;13:74–81.
[10] Petite H, Viateau V, Bensaid W, Meunier A, de Pollak C, Bourguignon M, et al. Tissue-engineered bone regeneration. Nat Biotechnol 2000;18:959–63.
[11] Siddappa R, Licht R, van Blitterswijk C, de Boer J. Donor variation and loss of multipotency during in vitro expansion of human mesenchymal stem cells for bone tissue engineering. J Orthop Res 2007;25:1029–41.
[12] Phinney DG, Kopen G, Righter W, Webster S, Tremain N, Prockop DJ. Donor variation in the growth properties and osteogenic potential of human marrow stromal cells. J Cell Biochem 1999;75:424–36.
[13] Oyajobi BO, Lomri A, Hott M, Marie PJ. Isolation and characterization of human clonogenic osteoblast progenitors immunoselected from fetal bone marrow stroma using STRO-1 monoclonal antibody. J Bone Miner Res 1999;14:351–61.

[14] Quirici N, Soligo D, Bossolasco P, Servida F, Lumini C, Deliliers GL. Isolation of bone marrow mesenchymal stem cells by anti-nerve growth factor receptor antibodies. Exp Hematol 2002;30:783–91.
[15] Sacchetti B, Funari A, Michienzi S, Di Cesare S, Piersanti S, Saggio I, et al. Self-renewing osteoprogenitors in bone marrow sinusoids can organize a hematopoietic microenvironment. Cell 2007;131:324–36.
[16] Dell'Accio F, De Bari C, Luyten FP. Molecular markers predictive of the capacity of expanded human articular chondrocytes to form stable cartilage in vivo. Arthritis Rheum 2001;44:1608–19.
[17] De Bari C, Dell'Accio F, Karystinou A, Guillot PV, Fisk NM, Jones EA, et al. A biomarker-based mathematical model to predict bone-forming potency of human synovial and periosteal mesenchymal stem cells. Arthritis Rheum 2008;58:240–50.
[18] Mendes SC, Tibbe JM, Veenhof M, Both S, Oner FC, van Blitterswijk CA, et al. Relation between in vitro and in vivo osteogenic potential of cultured human bone marrow stromal cells. J Mater Sci Mater Med 2004;15:1123–8.
[19] Larsen KH, Frederiksen CM, Burns JS, Abdallah BM, Kassem M. Identifying a molecular phenotype for bone marrow stromal cells with in vivo bone-forming capacity. J Bone Miner Res 2010;25:796–808.
[20] Burns JS, Rasmussen PL, Larsen KH, Schroder HD, Kassem M. Parameters in three-dimensional osteospheroids of telomerized human mesenchymal (stromal) stem cells grown on osteoconductive scaffolds that predict in vivo bone-forming potential. Tissue Eng Part A 2010;16:2331–42.
[21] Sontrop HMJ, Moerland PD, van den Ham R, Reinders MJT, Verhaegh WFJ. A comprehensive sensitivity analysis of microarray breast cancer classification under feature variability. BMC Bioinform 2009;10:389.
[22] Both SK, van der Muijsenberg AJC, van Blitterswijk CA, de Boer J, de Bruijn JD. A rapid and efficient method for expansion of human mesenchymal stem cells. Tissue Eng 2007;13:3–9.
[23] Yuan H, Van Den Doel M, Li S, Van Blitterswijk CA, De Groot K, De Bruijn JD. A comparison of the osteoinductive potential of two calcium phosphate ceramics implanted intramuscularly in goats. J Mater Sci Mater Med 2002;13:1271–5.
[24] Fernandes H, Mentink A, Bank R, Stoop R, van Blitterswijk C, de Boer J. Endogenous collagen influences differentiation of human multipotent mesenchymal stromal cells. Tissue Eng Part A 2010;16:1693–702.
[25] Mackay AM, Beck SC, Murphy JM, Barry FP, Chichester CO, Pittenger MF. Chondrogenic differentiation of cultured human mesenchymal stem cells from marrow. Tissue Eng 1998;4:415–28.
[26] Sekiya I, Colter DC, Prockop DJ. BMP-6 enhances chondrogenesis in a subpopulation of human marrow stromal cells. Biochem Biophys Res Commun 2001;284:411–8.
[27] Dellavalle A, Sampaolesi M, Tonlorenzi R, Tagliafico E, Sacchetti B, Perani L, et al. Pericytes of human skeletal muscle are myogenic precursors distinct from satellite cells. Nat Cell Biol 2007;9:255–67.
[28] Tusher VG, Tibshirani R, Chu G. Significance analysis of microarrays applied to the ionizing radiation response. Proc Natl Acad Sci U S A 2001;98:5116–21.
[29] Subramanian A, Tamayo P, Mootha VK, Mukherjee S, Ebert BL, Gillette MA, et al. Gene set enrichment analysis: a knowledge-based approach for interpreting genome-wide expression profiles. Proc Natl Acad Sci U S A 2005;102:15545–50.
[30] Van der Heijden F, Duin RPW, De Ridder D, Tax DMJ, Wiley J. PRTools version 4.0: a matlab toolbox for pattern recognition 2006.
[31] Waarsing JH, Day JS, van der Linden JC, Ederveen AG, Spanjers C, De Clerck N, et al. Detecting and tracking local changes in the tibiae of individual rats: a novel method to analyse longitudinal in vivo micro-CT data. Bone 2004;34:163–9.
[32] Fujita E, Kouroku Y, Ozeki S, Tanabe Y, Toyama Y, Maekawa M, et al. Oligo-astheno-teratozoospermia in mice lacking RA175/TSLC1/SynCAM/IGSF4A, a cell adhesion molecule in the immunoglobulin superfamily. Mol Cell Biol 2006;26:718–26.
[33] Dominici M, Le Blanc K, Mueller I, Slaper-Cortenbach I, Marini F, Krause D, et al. Minimal criteria for defining multipotent mesenchymal stromal cells. The international society for cellular therapy position statement. Cytotherapy 2006;8:315–7.
[34] Kratchmarova I, Blagoev B, Haack-Sorensen M, Kassem M, Mann M. Mechanism of divergent growth factor effects in mesenchymal stem cell differentiation. Science 2005;308:1472–7.
[35] Simonsen JL, Rosada C, Serakinci N, Justesen J, Stenderup K, Rattan SI, et al. Telomerase expression extends the proliferative life-span and maintains the osteogenic potential of human bone marrow stromal cells. Nat Biotechnol 2002;20:592–6.
[36] Meijer GJ, Mel P, Koole R, Cune MS. Fixed partial dentures on two implants: raising comfort in irradiated edentulous patients. Int J Oral Maxillofac Surg 2007;36:646–8.
[37] Zhang M, Xuan S, Bouxsein ML, von Stechow D, Akeno N, Faugere MC, et al. Osteoblast-specific knockout of the insulin-like growth factor (IGF) receptor gene reveals an essential role of IGF signaling in bone matrix mineralization. J Biol Chem 2002;277:44005–12.
[38] French DM, Kaul RJ, D'Souza AL, Crowley CW, Bao M, Frantz GD, et al. WISP-1 is an osteoblastic regulator expressed during skeletal development and fracture repair. Am J Pathol 2004;165:855–67.
[39] Li J, Sarosi I, Cattley RC, Pretorius J, Asuncion F, Grisanti M, et al. Dkk1-mediated inhibition of Wnt signaling in bone results in osteopenia. Bone 2006;39:754–66.
[40] Biederer T, Sara Y, Mozhayeva M, Atasoy D, Liu X, Kavalali ET, et al. SynCAM, a synaptic adhesion molecule that drives synapse assembly. Science 2002;297:1525–31.
[41] Lopez-Bendito G, Shigemoto R, Kulik A, Paulsen O, Fairen A, Lujan R. Expression and distribution of metabotropic GABA receptor subtypes GABABR1 and GABABR2 during rat neocortical development. Eur J Neurosci 2002;15:1766–78.
[42] Woronowicz A, Koshimizu H, Chang SY, Cawley NX, Hill JM, Rodriguiz RM, et al. Absence of carboxypeptidase E leads to adult hippocampal neuronal degeneration and memory deficits. Hippocampus 2008;18:1051–63.
[43] Wasaha S, Angelopoulos FM. What every woman should know about menopause. Am J Nurs 1996;96:24–32.
[44] Galuska SP, Rollenhagen M, Kaup M, Eggers K, Oltmann-Norden I, Schiff M, et al. Synaptic cell adhesion molecule SynCAM 1 is a target for polysialylation in postnatal mouse brain. Proc Natl Acad Sci U S A 2010;107:10250–5.
[45] Alves H, Munoz-Najar U, De Wit J, Renard AJ, Hoeijmakers JH, Sedivy JM, et al. A link between the accumulation of DNA damage and loss of multi-potency of human mesenchymal stromal cells. J Cell Mol Med 2010;14:2729–38.
[46] Singh S, Dhaliwal N, Crawford R, Xiao Y. Cellular senescence and longevity of osteophyte-derived mesenchymal stem cells compared to patient-matched bone marrow stromal cells. J Cell Biochem 2009;108:839–50.
[47] Meijer GJ, de Bruijn JD, Koole R, van Blitterswijk CA. Cell-based bone tissue engineering. PLoS Med 2007;4:e9.
[48] van Vliet MH, Klijn CN, Wessels LF, Reinders MJ. Module-based outcome prediction using breast cancer compendia. PLoS One 2007;2:e1047.
[49] Kuramochi M, Fukuhara H, Nobukuni T, Kanbe T, Maruyama T, Ghosh HP, et al. TSLC1 is a tumor-suppressor gene in human non-small-cell lung cancer. Nat Genet 2001;27:427–30.
[50] Ito A, Hagiyama M, Oonuma J. Nerve-mast cell and smooth muscle-mast cell interaction mediated by cell adhesion molecule-1, CADM1. J Smooth Muscle Res 2008;44:83–93.
[51] Hasstedt SJ, Bezemer ID, Callas PW, Vossen CY, Trotman W, Hebbel RP, et al. Cell adhesion molecule 1: a novel risk factor for venous thrombosis. Blood 2009;114:3084–91.
[52] Schmidmaier G, Wildemann B, Bail H, Lucke M, Fuchs T, Stemberger A, et al. Local application of growth factors (insulin-like growth factor-1 and transforming growth factor-beta1) from a biodegradable poly(D, L-lactide) coating of osteosynthetic implants accelerates fracture healing in rats. Bone 2001;28:341–50.
[53] Tamma R, Colaianni G, Zhu LL, DiBenedetto A, Greco G, Montemurro G, et al. Oxytocin is an anabolic bone hormone. Proc Natl Acad Sci U S A 2009;106:7149–54.
[54] Oliveira CS, Alves C. The role of the SHOX gene in the pathophysiology of Turner syndrome. Endocrinol Nutr 2011;58:433–42.
[55] Cobb J, Dierich A, Huss-Garcia Y, Duboule D. A mouse model for human short-stature syndromes identifies Shox2 as an upstream regulator of Runx2 during long-bone development. Proc Natl Acad Sci U S A 2006;103:4511–5.
[56] Vickerman L, Neufeld S, Cobb J. Shox2 function couples neural, muscular and skeletal development in the proximal forelimb. Dev Biol 2011;350:323–36.
[57] Drabek K, van de Peppel J, Eijken M, van Leeuwen JP. GPM6B regulates osteoblast function and induction of mineralization by controlling cytoskeleton and matrix vesicle release. J Bone Miner Res 2011;26:2045–51.
[58] Cheng Z, Tu C, Rodriguez L, Chen TH, Dvorak MM, Margeta M, et al. Type B gamma-aminobutyric acid receptors modulate the function of the extracellular Ca^{2+}-sensing receptor and cell differentiation in murine growth plate chondrocytes. Endocrinology 2007;148:4984–92.
[59] Djouad F, Delorme B, Maurice M, Bony C, Apparailly F, Louis-Plence P, et al. Microenvironmental changes during differentiation of mesenchymal stem cells towards chondrocytes. Arthritis Res Ther 2007;9:R33.
[60] Pennica D, Swanson TA, Welsh JW, Roy MA, Lawrence DA, Lee J, et al. WISP genes are members of the connective tissue growth factor family that are up-regulated in wnt-1-transformed cells and aberrantly expressed in human colon tumors. Proc Natl Acad Sci U S A 1998;95:14717–22.
[61] de Boer J, Siddappa R, Gaspar C, van Apeldoorn A, Fodde R, van Blitterswijk C. Wnt signaling inhibits osteogenic differentiation of human mesenchymal stem cells. Bone 2004;34:818–26.
[62] Chamorro MN, Schwartz DR, Vonica A, Brivanlou AH, Cho KR, Varmus HE. FGF-20 and DKK1 are transcriptional targets of beta-catenin and FGF-20 is implicated in cancer and development. EMBO J 2005;24:73–84.
[63] Banfi A, Muraglia A, Dozin B, Mastrogiacomo M, Cancedda R, Quarto R. Proliferation kinetics and differentiation potential of ex vivo expanded human bone marrow stromal cells: implications for their use in cell therapy. Exp Hematol 2000;28:707–15.
[64] Chatterjea A, Renard AJ, Jolink C, van Blitterswijk CA, de Boer J. Streamlining the generation of an osteogenic graft by 3D culture of unprocessed bone marrow on ceramic scaffolds. J Tissue Eng Regen Med 2012;6:103–12.

Please cite this article in press as: Mentink A, et al., Predicting the therapeutic efficacy of MSC in bone tissue engineering using the molecular marker CADM1, Biomaterials (2013), http://dx.doi.org/10.1016/j.biomaterials.2013.03.001